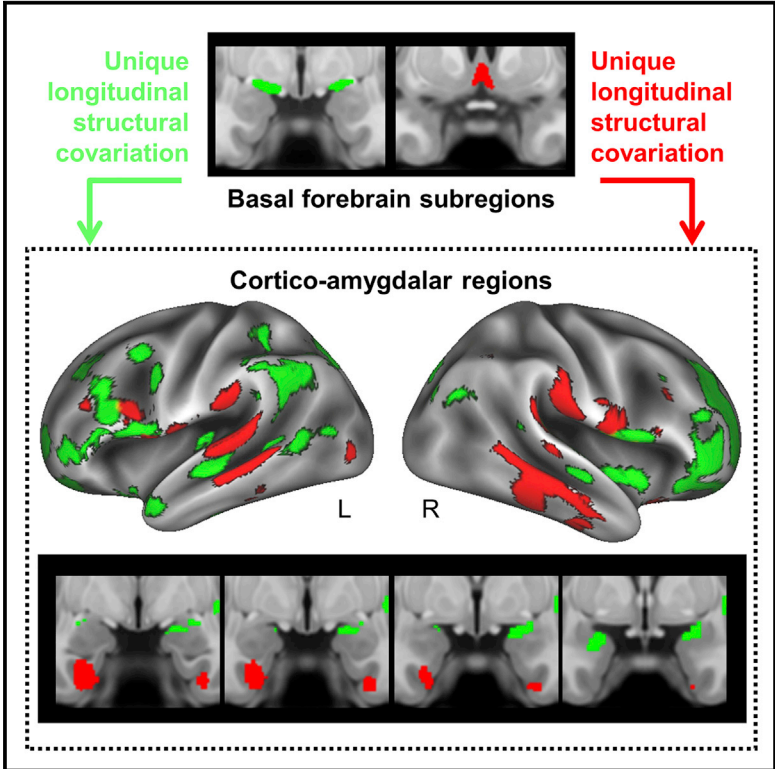# Cell Reports

Longitudinal Alzheimer's Degeneration Reflects the Spatial Topography of Cholinergic Basal Forebrain Projections

Graphical Abstract

Authors

Taylor W. Schmitz, Marieke Mur, Meghmik Aghourian, Marc-Andre Bedard, R. Nathan Spreng, for the Alzheimer's Disease Neuroimaging Initiative

Correspondence

taylor.schmitz@gmail.com

In Brief

Among older adults in prodromal stages of Alzheimer's disease, Schmitz et al. show that longitudinal degeneration within sub-regions of the basal forebrain covaries with cortico-amygdalar topographies of both structural degeneration and cholinergic denervation. The findings support the view that loss of cortico-amygdalar cholinergic input is a pivotal event in AD progression.

Highlights

- The basal forebrain degenerates substantially in early Alzheimer's disease (AD)

- Longitudinal gray matter loss in the basal forebrain, cortex, and amygdalae covaries

- This covariation reflects the organization of the basal forebrain cholinergic projections

- This covariation also reflects [18F] FEOBV PET indices of cholinergic denervation

CellPress

Longitudinal Alzheimer's Degeneration Reflects the Spatial Topography of Cholinergic Basal Forebrain Projections

Taylor W. Schmitz,[1,7,*] Marieke Mur,[2] Meghmik Aghourian,[3,4,5] Marc-Andre Bedard,[3,4,5] and R. Nathan Spreng[1,6] for the Alzheimer's Disease Neuroimaging Initiative

[1]Department of Neurology and Neurosurgery, Montreal Neurological Institute, McGill University, Montreal, QC, Canada
[2]Medical Research Council Cognition and Brain Sciences Unit, University of Cambridge, Cambridge, UK
[3]Cognitive Pharmacology Research Unit, Université du Québec à Montréal (UQAM), Montreal, QC, Canada
[4]McConnell Brain Imaging Centre, Montreal Neurological Institute, Montreal, QC, Canada
[5]McGill Centre for Studies in Aging, Douglas Mental Health University Institute, Verdun, QC, Canada
[6]Department of Human Development, Human Neuroscience Institute, Cornell University, Ithaca, NY, USA
[7]Lead Contact
*Correspondence: taylor.schmitz@gmail.com
https://doi.org/10.1016/j.celrep.2018.06.001

SUMMARY

The cholinergic neurons of the basal forebrain (BF) provide virtually all of the brain's cortical and amygdalar cholinergic input. They are particularly vulnerable to neuropathology in early Alzheimer's disease (AD) and may trigger the emergence of neuropathology in their cortico-amygdalar projection system through cholinergic denervation and *trans*-synaptic spreading of misfolded proteins. We examined whether longitudinal degeneration within the BF can explain longitudinal cortico-amygdalar degeneration in older human adults with abnormal cerebrospinal fluid biomarkers of AD neuropathology. We focused on two BF subregions, which are known to innervate cortico-amygdalar regions via two distinct macroscopic cholinergic projections. To further assess whether structural degeneration of these regions in AD reflects cholinergic denervation, we used the [18F] FEOBV radiotracer, which binds to cortico-amygdalar cholinergic terminals. We found that the two BF subregions explain spatially distinct patterns of cortico-amygdalar degeneration, which closely reflect their cholinergic projections, and overlap with [18F] FEOBV indices of cholinergic denervation.

INTRODUCTION

The emergence of Alzheimer's disease (AD) neuropathologies, such as misfolded β-amyloid (Aβ) and Tau proteins, progresses in stages across anatomically and functionally connected regions of the brain, with certain brain regions affected before others (Braak and Braak, 1991; Braak and Del Tredici, 2015; Raj et al., 2012, 2015; Seeley et al., 2009). Why certain brain regions appear more vulnerable to AD pathology than others has

long remained a mystery. However, recent functional genomics research, using brain tissue in both human AD and non-human animal models of AD, has started to elucidate structural and functional cell characteristics that predict selective neuronal vulnerability to AD pathology. Vulnerable neurons typically have large axonal projections that extend relatively long distances, from one region of the brain to another. As a result, they require high metabolic expenditure to maintain trophic support—transporting materials over long distances and maintaining enormous cytoskeletal surface areas. These morphological properties increase vulnerability to oxidative stress and neuroinflammation, perturbed energy homeostasis, and accumulation of misfolded proteins (Lewis et al., 2010; Mattson and Magnus, 2006; Wang et al., 2010).

The magnocellular cholinergic neurons in the basal forebrain (BF) are known to have very large projections, targeting distal areas of the cortical mantle and amygdalae via multiple routes such as the cingulum bundle (Bloem et al., 2014; Chandler et al., 2013; Hecker and Mesulam, 1994; Kondo and Zaborszky, 2016; Mesulam et al., 1983a, 1986; Zaborszky et al., 2015). Precise estimates of their size have been difficult to obtain due to the complexity of their axonal branching. Recently, however, the complete morphology of individual cholinergic neurons was visualized in mice using a novel cell labeling technique (Wu et al., 2014). Extrapolating from their results, the authors estimated that cholinergic projections in humans approach ~100 m in length for a single cell when accounting for all axonal branches. As a result of their exceptional size, cholinergic neurons are therefore likely to exhibit selective neuronal vulnerability (SNV) to AD pathology.

Consistent with the SNV model, post-mortem histological evidence suggests that the cholinergic BF neurons accumulate both intraneuronal Tau, and, interestingly, intraneuronal Aβ as early as the third decade of life, with profound accumulation observed 1 year after transition to mild cognitive impairment (MCI) (Arendt et al., 2015; Baker-Nigh et al., 2015; Braak and Braak, 1991; Braak and Del Tredici, 2015; Geula et al., 2008; Mesulam et al., 2004; Mesulam, 2013; Schliebs and Arendt, 2006, 2011). *In vivo* neuroimaging data have demonstrated that
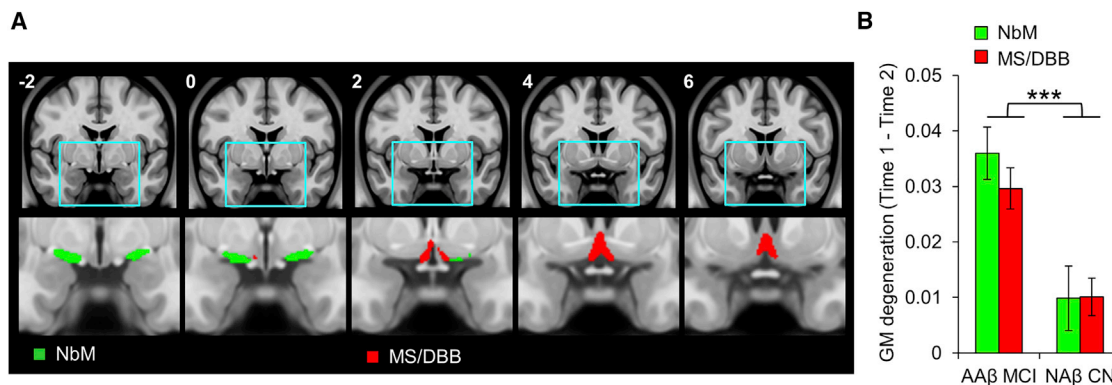
Figure 1. Basal Forebrain Regions of Interest and Longitudinal Degeneration in Early AD

(A) Regions of interest (ROIs) were defined from stereotaxic probabilistic maps of the human basal forebrain (Zaborszky et al., 2008). The nucleus basalis of Meynert (NbM) is displayed in green. The medial septal nucleus and diagonal band of Broca (MS/DBB) are displayed in red. The ROIs are projected on coronal slices in standard atlas space (MNI y coordinates are inset).

(B) Longitudinal degeneration (y axis) of both NbM and MS/DBB was elevated among individuals with abnormal cerebrospinal levels of the amyloid-β biomarker and mild cognitive impairment (AAβ MCI) relative to age-matched controls with normal Aβ and cognitive function (NAβ CN). y axis units are averaged gray matter volume within each ROI ± SEM.

cognitively normal (CN) older adults expressing abnormal cerebrospinal fluid (CSF) biomarkers of Aβ accumulation, i.e., individuals in preclinical stages of AD, exhibit greater longitudinal degeneration in the BF compared to CN adults with normal CSF Aβ (Schmitz and Spreng, 2016). Furthermore, total gray matter volume in the BF at baseline was found to predict subsequent longitudinal degeneration in the entorhinal cortex—a major target of cholinergic innervation (Kondo and Zaborszky, 2016)—and memory impairment. Competing models using baseline volume in entorhinal cortex to predict longitudinal degeneration in BF were not supported (Schmitz and Spreng, 2016). These findings suggest a potential interdependence between degeneration in the BF and the cholinoreceptive cortical targets of its projection system.

Research in non-human animals strongly supports this possibility. In mice bred to express a genetic knockout or knockdown of the vesicular acetylcholine transporter (VAChT, SLC18A3), a protein required for acetylcholine (ACh) release from cholinergic BF neurons (de Castro et al., 2009; Prado et al., 2013), long-term cholinergic deficiency leads to abnormal accumulation of Aβ and Tau in cholinoreceptive cortical neurons (Kolisnyk et al., 2016, 2017). These data suggest a role for cholinergic signaling in maintaining normal cell metabolism, including native biological functions related to the amyloid precursor and Tau proteins. In parallel to cholinergic denervation, intact but diseased cholinergic inputs might facilitate yet another mechanism of "seeding" the cortex with AD pathology, specifically through the *trans*-synaptic spread of misfolded Tau fragments (Clavaguera et al., 2009; de Calignon et al., 2012; Khan et al., 2014).

If the emergence of AD pathology in the cortex is caused by the loss of cortical cholinergic input or *trans*-synaptic spreading of Tau from cholinergic neurons, then the spatial topography of cortico-amygdalar degeneration should reflect the cholinergic projection system. The cholinergic BF projections exhibit topographical organization at multiple spatial scales (Ballinger et al., 2016; Bloem et al., 2014; Kondo and Zaborszky, 2016; Me-

sulam and Geula, 1988; Mesulam et al., 1983b, 1986; Zaborszky et al., 2015). To accommodate the spatial scale of high-resolution structural magnetic resonance imaging (MRI) data employed in the present study, we chose a topography that divides the BF into two segregated macroscopic projections (Zaborszky et al., 2008), the medial septal nucleus and diagonal band of Broca (MS/DBB) projection targeting medial temporal lobe, and the nucleus basalis of Meynert (NbM) projection targeting frontoparietal cortices and the amygdalae (Figures 1A and S1; Experimental Procedures). Structural properties such as gray matter volume are known to selectively co-vary between brain regions that are functionally and anatomically connected (Alexander-Bloch et al., 2013; Bassett et al., 2008; Cantero et al., 2017; Chen et al., 2008; Dupre and Spreng, 2017; He et al., 2007; Kilimann et al., 2017; Schmitz and Spreng, 2016; Spreng and Turner, 2013), enabling us to test the covariance in longitudinal structural degeneration between the BF and distinct targets of its cholinergic projections in the cortex and amygdalae.

Longitudinal voxel-based morphometry was used to measure changes in BF and cortico-amygdalar gray matter (GM) volume over a 2-year interval in older adults with mild cognitive impairment (MCI) and the CSF-Aβ biomarker of central AD pathology (Shaw et al., 2009). These data were acquired from the Alzheimer's Disease Neuroimaging Initiative (Mueller et al., 2005). Voxel-based morphometry was used to derive longitudinal indices of GM degeneration within the BF sub-regions (Grothe et al., 2018). We then performed a "seed-to-searchlight" analysis to determine whether the BF MS/DBB and NbM sub-regions (the "seeds") exhibit unique patterns of covariation with regions of cortex (the "searchlights"). We then compared these maps against a direct *in vivo* assay of cortical cholinergic denervation using the positron emission tomography (PET) radiotracer [18F] FEOBV, which exhibits high binding sensitivity and specificity to VAChT (Aghourian et al., 2017). We show that in AD, topographies of longitudinal cortical degeneration covary with
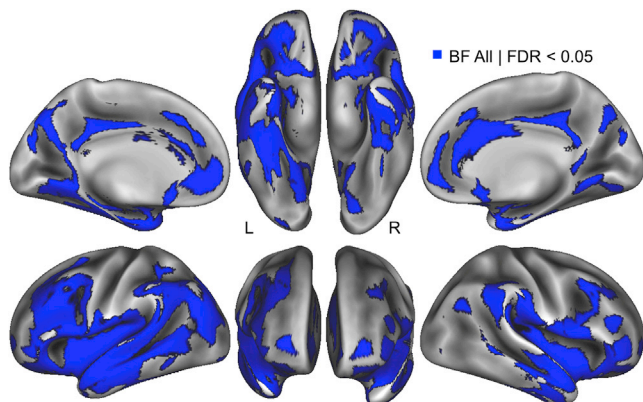
■ BF All | FDR < 0.05

L   R

Figure 2. Spatial Topography of Covariance between BF and Cortical Degeneration

Seed-to-searchlight analysis tested whether BF degeneration (averaged over NbM and MS/DBB sub-regions) covaried with cortical degeneration within 6 mm radius spherical "searchlight" ROIs in the AAβ MCI group, controlling for age, sex, education, total intracranial volume, and longitudinal change in whole brain volume. Significant searchlights (blue overlay) were determined using a false discovery rate (FDR)-corrected p < 0.05. Results are projected on an inflated cortical surface in MNI atlas space.

longitudinal degeneration of the NbM and MS/DBB and closely reflect the known anatomical organization of the cortical cholinergic projection system, as well as the functional topographies of cortical cholinergic denervation assayed by [^{18}F] FEOBV PET.

RESULTS

The BF Exhibits Severe Longitudinal Degeneration in Early AD

To ensure the presence of AD pathology in our sample of older adults, independent of longitudinal structural MRI, we used the cerebrospinal fluid amyloid-β biomarker (CSF Aβ$_{1-42}$). Prior analyses of the ADNI core datasets (Shaw et al., 2009) have provided a cutpoint for CSF Aβ$_{1-42}$ concentration at which diagnostic sensitivity and specificity to AD is maximal (192 pg mL^{-1}), yielding correct detection of 96.4% (<192 pg mL^{-1}) and correct rejection of 95.2% (>192 pg mL^{-1}) (Experimental Procedures). Only individuals with abnormal CSF Aβ$_{1-42}$ values (AAβ) falling below this cutpoint were included. Second, in order to ensure our sample was at a stage of AD characterized by longitudinal degeneration in amygdalar, allocortical, and neocortical areas (Grothe et al., 2013; Schmitz and Spreng, 2016), we further filtered individuals according to their neuropsychological status. Only individuals with a diagnosis of MCI based on the ADNI neuropsychological test battery were included. We included both MCI individuals who remained stable and converted to AD in the 2-year study interval. After triangulating AD pathology from CSF biomarker and neuropsychological measures, our final sample size of AAβ MCI adults was n = 80 (mean ± SD; CSF Aβ$_{1-42}$ concentration = 136.45 ± 25.31, range = 81–190). See Table S1 for demographic and neuropsychological information, as well as CSF total Tau and phosphorylated Tau indices. See Table S2 for individual ADNI research identifier numbers, sMRI image identifier numbers, and Aβ subgroup designation. Individ-

uals presenting MCI neuropsychological status but normal CSF Aβ levels were excluded from all forthcoming analyses, as their cognitive symptoms are likely to be caused by non-AD pathology, for example, vascular dementia and hippocampal sclerosis. See Table S3 for excluded MCI participants.

We next confirmed that the AAβ MCI group exhibited abnormal longitudinal degeneration in the BF subregional ROIs: NbM and MS/DBB. To do so, we compared longitudinal GM changes (time 1 – time 2) in the AAβ MCI group against a control group of age-matched older adults with both normal CSF Aβ$_{1-42}$ values (NAβ) and normal neuropsychological status (NAβ CN: n = 52, mean ± SD; CSF Aβ$_{1-42}$ concentration = 242.46 ± 25.55, range = 196–300). These groups also differed significantly in their CSF concentrations of total Tau and phosphorylated Tau (Tables S1 and S2). A 2 (group) × 2 (BF ROI) repeated-measures ANOVA revealed a significant main effect of group (F$_{1,130}$ = 16.4, p < 0.001), driven by significant between group differences in both BF subregions (NbM: t$_{130}$ = 3.5, p < 0.001; MS/DBB: t$_{130}$ = 3.9, p < 0.001) (Figure 1B). We did not observe a main effect of ROI (F < 1), or a group by ROI interaction (F = 1). Consistent with existing work on longitudinal structural degeneration of the BF in MCI (Grothe et al., 2013; Schmitz and Spreng, 2016), our initial findings indicate that the presence of AD pathology yielded large increases in the magnitude of degeneration in both BF nuclei over a 2-year interval compared to normally aging older adults.

Covariation of Longitudinal Degeneration between the BF and Cortico-Amygdalar Regions

Having confirmed abnormal BF degeneration in our MCI sample, we next conducted a regression-based seed-to-searchlight analysis using the entire BF (NbM and MS/DBB combined) as the seed region. Searchlight analyses test a statistical model in small spherical ROIs ("searchlights") centered on every voxel, as opposed to the individual voxels themselves (Kriegeskorte et al., 2006). At each searchlight, a multiple linear regression model was performed with mean longitudinal degeneration (time 1 – time 2) within the BF as the predictor, and nuisance covariates for age, sex, education, total intracranial volume, and longitudinal change in whole brain volume. The dependent variable was mean degeneration (time 1 – time 2) within the cortical searchlight. A significant searchlight indicates a covariation in longitudinal degeneration between the BF and the local neighborhood of voxels within the searchlight region.

Across AAβ MCI individuals, we found that larger magnitudes of longitudinal BF degeneration covaried with larger magnitudes of cortical degeneration in the frontal, temporal, and parietal cortices. The data were corrected for multiple comparisons using a false discovery (FDR) rate p < 0.05 (Figure 2). Spatial foci within these cortical areas are in close agreement with prior work showing preferential vulnerability to AD pathology in anterior medial temporal cortex, cingulate cortex, and lateral frontoparietal cortices (Buckner et al., 2005). We also observed significant covariation bilaterally in the amygdalae.

We conducted a second seed-to-searchlight analysis in the NAβ CN group, using the same model specifications as in the AAβ MCI group. However, this model failed to detect suprathreshold cortical degeneration after correction for multiple
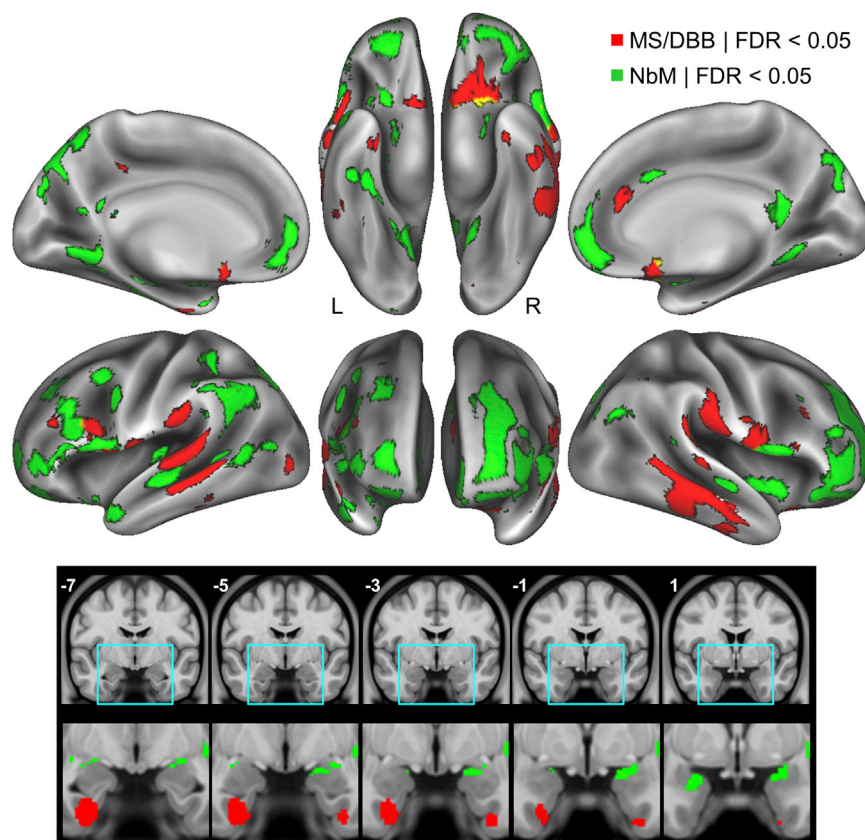
Figure 3. Degeneration within BF NbM and MS/DBB Nuclei Covaries with Distinct Spatial Topographies of Degeneration in Their Cortical Targets

Seed-to-searchlight analysis tested whether the NbM or MS/DBB BF subregions selectively covaried with cortical degeneration in the AAβ MCI group, controlling for degeneration in the opposing BF subregion (MS/DBB and NbM, respectively). The NbM selectively covaried with degeneration (green overlays) in distributed areas of frontal, parietal, and occipital cortex (top), as well as in the amygdalae (bottom). The MS/DBB selectively covaried with degeneration (red overlays) in more circumscribed areas of temporal cortex including the middle temporal gyrus (cortical surfaces), and the entorhinal cortices (bottom). Additional areas included the temporo-parietal and left inferior frontal cortices. Significant searchlights were determined using a FDR-corrected p < 0.05. Top: results are projected on an inflated cortical surface in MNI atlas space. Bottom: results are displayed on coronal slices in MNI atlas space (y coordinates are inset).

comparisons. Hence, these patterns do not appear to reflect normal age-related patterns of covariance between BF and cortical degeneration.

Cortico-Amygdalar Covariation with BF Subregions Reflects the Cholinergic BF Projections

Many of the spatial foci identified by this initial analysis are also known to be strongly innervated by the ascending cholinergic projections, including the entorhinal cortex, hippocampus, amygdalae, and medial prefrontal cortex (Bloem et al., 2014; Chandler et al., 2013; Hecker and Mesulam, 1994; Kondo and Zaborszky, 2016; Mesulam et al., 1986, 1983a; Zaborszky et al., 2015). However, the observed spatial topography may merely reflect coincidental degeneration of the BF, cortex, and amygdalae; AAβ MCI individuals with larger magnitudes of BF degeneration may tend to exhibit larger magnitudes of cortico-amygdalar degeneration due to parallel independent events. If this were the case, we would not expect degeneration within subregions of the BF to exhibit distinct patterns of covariation with degeneration in the cortex and amygdalae. Alternatively, if pathological events within the cholinergic BF subregions and their cortico-amygdalar targets are linked, longitudinal degeneration in NbM and MS/DBB should exhibit a pattern of cortico-amygdalar interdependence reflecting the distinct topography of their projections.

To adjudicate these competing alternatives, we conducted two modified seed-to-searchlight analyses on each BF subre-

gion—NbM and MS/DBB—that are known to form segregated macroscopic projections to distinct areas of cortex and amygdalae. Each analysis examined whether mean longitudinal degeneration (time 1 – time 2) within either the NbM or MS/DBB ROI selectively covaried with mean degeneration within the cortical searchlights, while controlling for degeneration in the opposing subregion. As before, additional covariates included age, sex, education, total intracranial volume, and longitudinal change in whole brain volume.

Across AAβ MCI individuals, we observed that NbM and MS/DBB selectively covaried with distinct topographies of cortical degeneration that closely align with the segregated organization of their cholinergic projections (Figure 3). Higher magnitudes of NbM degeneration selectively covaried with higher magnitudes of degeneration in a more distributed topography reflecting its widespread cholinergic innervations of the frontal, parietal, and occipital cortices (Bloem et al., 2014; Mesulam and Geula, 1988; Mesulam et al., 1986, 1983a). The NbM also selectively covaried with higher focal degeneration in the amygdalae, an area which is densely innervated by its cholinergic projections (Hecker and Mesulam, 1994).

By contrast, the MS/DBB selectively covaried with higher magnitudes of degeneration in a more circumscribed topography. Degeneration within the temporal lobe, including the entorhinal cortex and extending laterally into the middle temporal gyri, are areas known to receive cholinergic innervations from the medial septal nucleus (MS) and vertical band of the DBB (Kondo and Zaborszky, 2016). Areas of MS/DBB covariation outside of the temporal cortex included the olfactory cortex, an area known to receive cholinergic projections from the horizontal band of the DBB (Mesulam et al., 1983a, 1986). Our longitudinal findings are consistent with cross-sectional studies
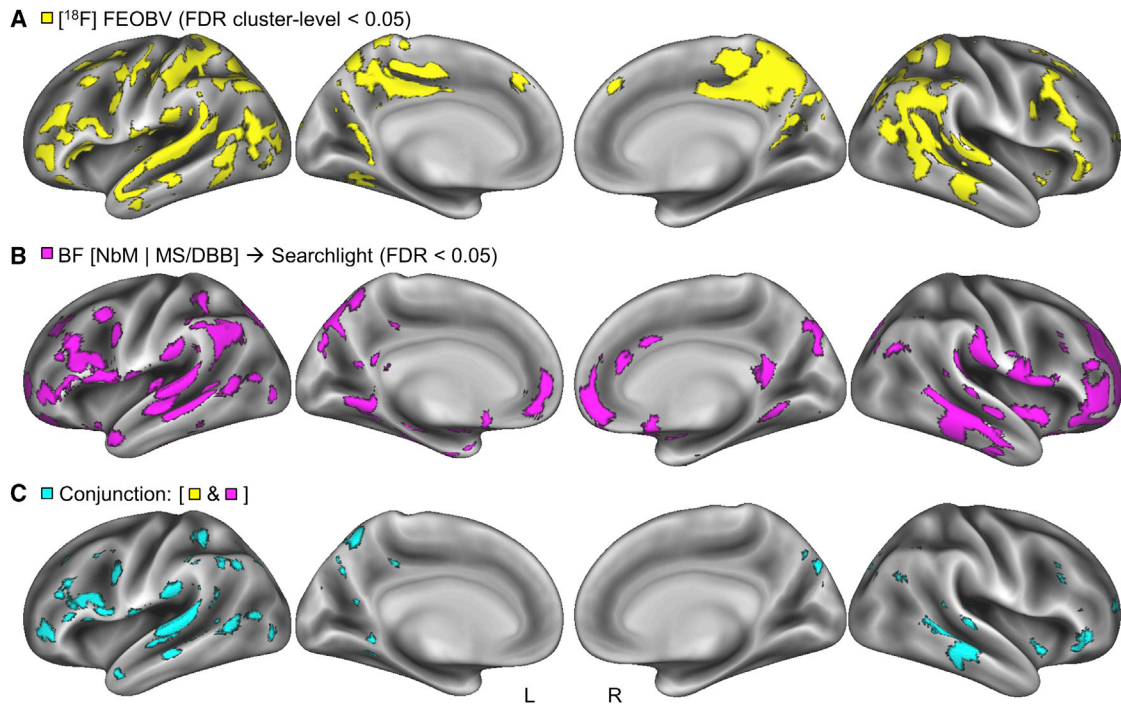
Figure 4. Spatial Convergence across Multimodal Indices of Cortical Cholinergic Degeneration
(A) A map of cortical cholinergic degeneration assayed by between group comparison of [^{18}F] FEOBV binding in cognitively normal versus AD adults (primary cluster forming threshold p uncorrected <0.001, secondary FDR cluster level threshold <0.05).
(B) A composite of the seed-to-searchlight maps for each BF subregion (Figure 3) was generated using a logical OR operation.
(C) A conjunction analysis (logical AND) was then applied to the FDR-corrected maps in (A) and (B). Results are projected on an inflated cortical surface in MNI atlas space.

demonstrating stronger inter-regional covariation of MS/DBB with hippocampal and amygdalar gray matter, and NbM with cingulate gray matter, in MCI compared to CN older adults (Cantero et al., 2017; Kilimann et al., 2017).

The subregional NbM and MS/DBB searchlight topographies were more spatially restricted than the searchlight topography observed in the initial analysis (both NbM and MS/DBB combined; Figure 2), especially in the cortical midline, indicating that the NbM and MS/DBB share common variance in these searchlight locations.

Convergent Structural and Functional Topographies of Cholinergic Degeneration

Our seed-to-searchlight structural degeneration maps suggest an interdependence between AD pathology within the BF projection system and its cortico-amygdalar targets. However, by itself, sMRI cannot determine whether the observed structural interdependencies (Figure 3) are specific to cortical cholinergic innervations. We therefore adopted a multimodal imaging strategy using the [^{18}F] FEOBV PET radiotracer, which exhibits a very high binding affinity and an excellent specificity for the vesicular acetylcholine transporter (VAChT), a glycoprotein found on the membrane of synaptic vesicles of cholinergic neurons (Aghourian et al., 2017; Cyr et al., 2014; Parent et al., 2012) (Figure S2; Table S4; Supplemental Experimental Procedures). The [^{18}F] FEOBV tracer provides an estimate of presynaptic neuronal

integrity and is thought to remain unaffected by the post-synaptic activity of enzymes such as acetylcholinesterase (ACHE), although this has yet to be demonstrated *in vivo*. Cortical cholinergic denervation, whether induced experimentally via selective lesions of the BF nuclei in rats (Cyr et al., 2014; Parent et al., 2012), or due to AD pathology in humans (Aghourian et al., 2017), both alter regionally specific patterns of [^{18}F] FEOBV binding.

We first compared cognitively normal (n = 6) and AD (n = 6) older adults with indices of [^{18}F] FEOBV PET, collected as part of a prior study (Aghourian et al., 2017), to identify areas of significant cholinergic denervation. A two-sample t test controlling for age (Table S4; Experimental Procedures) revealed lower [^{18}F] FEOBV binding in the AD group spanning lateral fronto-parietal and temporal cortical areas. Due to the smaller sample sizes, we first imposed a cluster-forming threshold with an uncorrected p < 0.001, followed a cluster-level FDR-corrected p < 0.05 (Woo et al., 2014) (Figure 4A). We note that no differences were observed in the thalamus, medial temporal lobe, or amygdalar areas at the FDR-corrected threshold.

We next examined the precise areas of spatial convergence between the [^{18}F] FEOBV assay of cholinergic denervation (Figure 4A) and our seed-to-searchlight assay of BF-dependent structural degeneration (Figure 4B). To do so, a logical AND operation was performed on the FDR-corrected maps from each imaging modality (Nichols et al., 2005). The resulting

conjunction revealed tight correspondence in virtually all cortical areas of the left hemisphere. The right hemisphere exhibited lower spatial overlap, due in part to weaker effect sizes of clusters in these areas in the [18F] FEOBV group comparison (Figure 4C). Taken together, these findings indicate that spatial topographies of cortical degeneration in AD reflect the anatomical topography of the cholinergic projection system, and thus suggest the loss of cortical cholinergic input from the BF might play a major role in the emergence of cortico-amygdalar gray matter degeneration.

DISCUSSION

We demonstrated that the MS/DBB and NbM subregions of the basal forebrain covary with segregated topographies of cortical degeneration (Figure 3). These topographies align closely with the known anatomical segregation between the cholinergic projections of the MS/DBB and NbM subregions (Bloem et al., 2014; Hecker and Mesulam, 1994; Kondo and Zaborszky, 2016; Mesulam et al., 1983a, 1986; Zaborszky et al., 2015). We then used [18F] FEOBV PET indices of binding with the vesicular acetylcholine transporter (VAChT) to demonstrate that cortical cholinergic denervation in AD exhibits spatial correspondence with our BF-dependent structural degeneration maps (Figure 4).

If the cholinergic BF neurons are selectively vulnerable to perturbed energy homeostasis, oxidative stress, and neuroinflammation due to their large axons (Lewis et al., 2010; Mattson and Magnus, 2006; Wang et al., 2010; Wu et al., 2014), they might lose the capacity to maintain full trophic support of these large axons over the course of aging. Lending support to this hypothesis, the number of cholinergic fibers per BF neuron reduces in early middle age, and especially in the transition from preclinical to MCI stages of AD, against a background of accumulating intraneuronal Aβ, hyper-phosphorylated Tau, and neurofibrillary tangles (Arendt et al., 2015; Baker-Nigh et al., 2015; Braak and Braak, 1991; Braak and Del Tredici, 2015; Geula et al., 2008; Mesulam et al., 2004; Mesulam, 2013; Schliebs and Arendt, 2006, 2011). As a result, the cortex and amygdalae might become progressively denuded of cholinergic input, with genetic AD risk factors such as the APOE ε4 allele (Poirier et al., 1995) and reduced metabolism (Rivera et al., 2005) contributing to differentiate normal age-related from AD trajectories of cholinergic loss.

Work in non-human animals indicates that cortico-amygdalar cholinergic denervation is a pivotal event in the AD pathophysiological cascade. Among mice bred to express a deficiency in VAChT (SLC18A3) capacity, the consequent reduction in cholinergic tone across the lifespan is, by itself, sufficient to induce aggregation of Aβ and hyper-phosphorylated Tau within brain areas receiving BF cholinergic projections, such as the hippocampus (Kolisnyk et al., 2016, 2017). Under this scenario, loss of cholinergic BF projections might "seed" pathophysiological changes in their cortical and amygdalar targets due to loss of cholinergic signaling. In parallel to the loss of cholinergic input, intact but diseased cholinergic projections might also transmit Tau trans-synaptically to cholinoreceptvie cortico-amygdalar neurons. Trans-synaptic spread of Tau has been reported for glutamatergic neurons in the entorhinal and hippocampal cortices (Clavaguera et al., 2009; de Calignon et al., 2012;

Khan et al., 2014), however, the findings imply a general mechanism by which AD pathology can spread from diseased neurons to functionally and anatomically connected healthy neurons. In either scenario, degeneration within cortico-amygdalar targets of cholinergic BF projections should reflect the topography of the cholinergic projections themselves. We provide additional support for this hypothesis with longitudinal structural MRI.

In humans, cholinergic hypofunction correlates with the formation of Aβ plaques, tangles containing hyper-phosphorylated Tau and clinical severity of AD (Auld et al., 2002; Fisher, 2012). We observed that in addition to abnormal CSF Aβ concentration (that was used as a grouping variable), both CSF phosphorylated Tau and total Tau were significantly elevated in the AAβ MCI compared to the NAβ CN group (Table S1). Although we cannot infer from CSF data where and how these biomarkers are distributed in the brain, our findings demonstrate that in the MCI group longitudinal gray matter degeneration within the cortico-amygdalar cholinergic BF projection system, as well as cognitive decline, occurred against a biomolecular background of significant neuropathology. Nevertheless, in humans, stronger connections are needed to link the progression of cortical cholinergic denervation to its potentially very early roles in driving cortical neuropathology and altering cortical functions important for cognition, such as selective attention (Romberg et al., 2013; Schmitz et al., 2010, 2014; Schmitz and Duncan, 2018).

Standard T1-weighted sMRI measures of gray matter volume cannot distinguish different cell types. Hence, we cannot infer from our sMRI data alone whether longitudinal reductions in gray matter within the BF reflect a selective loss of cholinergic cell bodies, or some combination of cholinergic, GABAergic, and glutamatergic neurons known to co-populate its MS/DBB and NbM subregions (Henny and Jones, 2008; Lin et al., 2015). The [18F] FEOBV PET radiotracer obviates this limitation. Unlike FDG and amyloid radiotracers, [18F] FEOBV provides a highly sensitive and selective biomarker of central cholinergic integrity—VAChT binding (Aghourian et al., 2017). In the present study, we did not have access to longitudinal structural MRI and [18F] FEOBV PET within the same individuals. Although we assessed the spatial convergence between imaging modalities using conjunction analysis in MNI template space, the accuracy of co-registration between modalities can be further improved by acquiring high-resolution PET and structural MRI within the same individuals. Finally, we note that [18F] FEOBV PET was acquired in AD participants who were actively taking ACHE inhibitors to treat cognitive symptoms. Systematic investigation is required to determine whether these drugs might influence [18F] FEOBV binding.

Future work will benefit from a within-subjects multimodal imaging strategy combining longitudinal [18F] FEOBV PET with structural MRI, as well as direct evaluation of how pharmacological intervention with ACHE inhibitors influences these measures. Nevertheless, our present findings underscore the need for in vivo measures of cell-type-specific degeneration of the cholinergic system. Longitudinal monitoring of [18F] FEOBV binding in cohorts of cognitively normal APOE ε4 carriers and non-carriers, in combination with CSF biomarker indices of neuropathology, will provide novel insights into the differential trajectories of the neurotypical and preclinical aging brain.

EXPERIMENTAL PROCEDURES

Structural MRI

Data used in the preparation of this article were obtained from the Alzheimer's Disease Neuroimaging Initiative (ADNI) database (http://adni.loni.usc.edu). The ADNI was launched in 2003 as a public-private partnership, led by Principal Investigator Michael W. Weiner, MD. The primary goal of ADNI has been to test whether serial magnetic resonance imaging (MRI), positron emission tomography (PET), cerebrospinal fluid (CSF) biomarkers, and clinical and neuropsychological assessment can be combined to measure the progression of mild cognitive impairment (MCI) and early Alzheimer's disease (AD).

Methodological steps for group classification (cognitively normal and early AD), structural MRI preprocessing, and definition of basal forebrain ROIs are in the Supplemental Information.

Seed-to-Searchlight Analyses

Longitudinal differences in GM were computed for the combined BF (NbM, MS/DBB) ROI and the NbM and MS/DBB sub-region ROIs, for each subject. These values were entered into multiple linear regression models (either combined BF only, or both NbM and MD/DBB) as the predictor "seeds." In both cases, additional covariates included: age, sex, education, total intracranial volume, and longitudinal change in whole brain volume. The dependent measure was the longitudinal difference in GM within a 6-mm radius spherical searchlight ROI. Over successive iterations, the searchlight was positioned at every voxel constrained within the population-average gray matter mask, producing a seed-to-searchlight map. At each searchlight the multiple linear regression was computed with the robust fitting method (i.e., robust regression) (Wilcox, 2004) to reduce potential outlier effects. Code for the seed-to-searchlight analyses was adapted from the freely available RSA Toolbox (Nili et al., 2014). Statistical significance on the searchlight maps was determined at a FDR-corrected $p < 0.05$.

[18]F FEOBV PET

The [18F] FEOBV PET radiotracer was acquired in 12 participants: six patients diagnosed with probable AD and six age-matched healthy volunteers (Table S4). These sample sizes are similar to those of previous rodent studies comparing FEOBV binding between an experimental group with induced mild cholinergic lesions and controls (Cyr et al., 2014; Parent et al., 2012). All participants were recruited at the McGill Centre for Studies in Aging (MCSA) and assessed at the McConnell Brain Imaging Unit (BIC) of the Montreal Neurological Institute (MNI). The original study protocol was approved by "Université du Québec à Montréal" (UQAM), and McGill University Research Ethics Boards. Informed consent was obtained from all subjects prior to participation in the study.

Methodological steps for group classification (cognitively normal and early AD) and [18F] FEOBV PET preprocessing are in the Supplemental Information.

ANCOVA Model

We used SPM12 (http://www.fil.ion.ucl.ac.uk/spm/software/spm12/) to conduct a between groups analysis (CN versus AD). The parameters for the general linear model specification were as follows: threshold masking = relative (0.8), global calculation = mean voxel value, global normalization = overall grand mean scaling (50); normalization = ANCOVA. Other parameter fields were set to default values. Age was modeled as a covariate of non-interest in the model. Statistical significance on the between group contrast (CN > AD) was determined at a cluster-level FDR-corrected $p < 0.05$.

SUPPLEMENTAL INFORMATION

Supplemental Information includes Supplemental Experimental Procedures, two figures, and four tables and can be found with this article online at https://doi.org/10.1016/j.celrep.2018.06.001.

ACKNOWLEDGMENTS

AUTHOR CONTRIBUTIONS

ADNI collected all data, with the exception of the [18F] FEOBV PET experiments, which were collected by M.A. and M.-A.B. The ADNI data were preprocessed by R.N.S. The [18F] FEOBV PET data were preprocessed by M.A. and M.-A.B. All additional analyses on the ADNI and [18F] FEOBV PET data were conducted by T.W.S. and M.M. T.W.S. and R.N.S. wrote the paper, with the exception of the [18F] FEOBV PET methods (M.A. and M.-A.B.).

DECLARATION OF INTERESTS

The authors declare no competing interests.

REFERENCES

Aghourian, M., Legault-Denis, C., Soucy, J.P., Rosa-Neto, P., Gauthier, S., Kostikov, A., Gravel, P., and Bédard, M.A. (2017). Quantification of brain cholinergic denervation in Alzheimer's disease using PET imaging with [18F]-FEOBV. Mol. Psychiatry 22, 1531–1538.

Alexander-Bloch, A., Giedd, J.N., and Bullmore, E. (2013). Imaging structural co-variance between human brain regions. Nat. Rev. Neurosci. 14, 322–336.

Arendt, T., Brückner, M.K., Morawski, M., Jäger, C., and Gertz, H.J. (2015). Early neurone loss in Alzheimer's disease: cortical or subcortical? Acta Neuropathol. Commun. 3, 10.

Auld, D.S., Kornecook, T.J., Bastianetto, S., and Quirion, R. (2002). Alzheimer's disease and the basal forebrain cholinergic system: relations to beta-amyloid peptides, cognition, and treatment strategies. Prog. Neurobiol. 68, 209–245.

Baker-Nigh, A., Vahedi, S., Davis, E.G., Weintraub, S., Bigio, E.H., Klein, W.L., and Geula, C. (2015). Neuronal amyloid-β accumulation within cholinergic basal forebrain in ageing and Alzheimer's disease. Brain 138, 1722–1737.

Ballinger, E.C., Ananth, M., Talmage, D.A., and Role, L.W. (2016). Basal forebrain cholinergic circuits and signaling in cognition and cognitive decline. Neuron 91, 1199–1218.

Bassett, D.S., Bullmore, E., Verchinski, B.A., Mattay, V.S., Weinberger, D.R., and Meyer-Lindenberg, A. (2008). Hierarchical organization of human cortical networks in health and schizophrenia. J. Neurosci. 28, 9239–9248.

Bloem, B., Schoppink, L., Rotaru, D.C., Faiz, A., Hendriks, P., Mansvelder, H.D., van de Berg, W.D., and Wouterlood, F.G. (2014). Topographic mapping between basal forebrain cholinergic neurons and the medial prefrontal cortex in mice. J. Neurosci. 34, 16234–16246.

Braak, H., and Braak, E. (1991). Neuropathological stageing of Alzheimer-related changes. Acta Neuropathol. 82, 239–259.

Braak, H., and Del Tredici, K. (2015). The preclinical phase of the pathological process underlying sporadic Alzheimer's disease. Brain 138, 2814–2833.

Buckner, R.L., Snyder, A.Z., Shannon, B.J., LaRossa, G., Sachs, R., Fotenos, A.F., Sheline, Y.I., Klunk, W.E., Mathis, C.A., Morris, J.C., and Mintun, M.A. (2005). Molecular, structural, and functional characterization of Alzheimer's disease: evidence for a relationship between default activity, amyloid, and memory. J. Neurosci. 25, 7709–7717.

Cantero, J.L., Zaborszky, L., and Atienza, M. (2017). Volume loss of the nucleus basalis of Meynert is associated with atrophy of innervated regions in mild cognitive impairment. Cereb. Cortex 27, 3881–3889.

Chandler, D.J., Lamperski, C.S., and Waterhouse, B.D. (2013). Identification and distribution of projections from monoaminergic and cholinergic nuclei to functionally differentiated subregions of prefrontal cortex. Brain Res. 1522, 38–58.

Chen, Z.J., He, Y., Rosa-Neto, P., Germann, J., and Evans, A.C. (2008). Revealing modular architecture of human brain structural networks by using cortical thickness from MRI. Cereb. Cortex 18, 2374–2381.

Clavaguera, F., Bolmont, T., Crowther, R.A., Abramowski, D., Frank, S., Probst, A., Fraser, G., Stalder, A.K., Beibel, M., Staufenbiel, M., et al. (2009). Transmission and spreading of tauopathy in transgenic mouse brain. Nat. Cell Biol. 11, 909–913.

Cyr, M., Parent, M.J., Mechawar, N., Rosa-Neto, P., Soucy, J.P., Aliaga, A., Kostikov, A., Maclaren, D.A., Clark, S.D., and Bedard, M.A. (2014). PET imaging with [18F]fluoroethoxybenzovesamicol ([18F]FEOBV) following selective lesion of cholinergic pedunculopontine tegmental neurons in rat. Nucl. Med. Biol. 41, 96–101.

de Calignon, A., Polydoro, M., Suárez-Calvet, M., William, C., Adamowicz, D.H., Kopeikina, K.J., Pitstick, R., Sahara, N., Ashe, K.H., Carlson, G.A., et al. (2012). Propagation of tau pathology in a model of early Alzheimer's disease. Neuron 73, 685–697.

de Castro, B.M., De Jaeger, X., Martins-Silva, C., Lima, R.D., Amaral, E., Menezes, C., Lima, P., Neves, C.M., Pires, R.G., Gould, T.W., et al. (2009). The vesicular acetylcholine transporter is required for neuromuscular development and function. Mol. Cell. Biol. 29, 5238–5250.

Dupre, E., and Spreng, R.N. (2017). Structural covariance networks across the lifespan, from 6 to 94 years of age. Netw. Neurosci. 1, 302–323.

Fisher, A. (2012). Cholinergic modulation of amyloid precursor protein processing with emphasis on M1 muscarinic receptor: perspectives and challenges in treatment of Alzheimer's disease. J. Neurochem. 120 (Suppl 1), 22–33.

Geula, C., Nagykery, N., Nicholas, A., and Wu, C.K. (2008). Cholinergic neuronal and axonal abnormalities are present early in aging and in Alzheimer disease. J. Neuropathol. Exp. Neurol. 67, 309–318.

Grothe, M., Heinsen, H., and Teipel, S. (2013). Longitudinal measures of cholinergic forebrain atrophy in the transition from healthy aging to Alzheimer's disease. Neurobiol. Aging 34, 1210–1220.

Grothe, M., Kilimann, I., Grinberg, L., Heinsen, H., and Teipel, S. (2018). In vivo volumetry of the cholinergic basal forebrain. Neuromethods, 213–232.

He, Y., Chen, Z.J., and Evans, A.C. (2007). Small-world anatomical networks in the human brain revealed by cortical thickness from MRI. Cereb. Cortex 17, 2407–2419.

Hecker, S., and Mesulam, M.M. (1994). Two types of cholinergic projections to the rat amygdala. Neuroscience 60, 383–397.

Henny, P., and Jones, B.E. (2008). Projections from basal forebrain to prefrontal cortex comprise cholinergic, GABAergic and glutamatergic inputs to pyramidal cells or interneurons. Eur. J. Neurosci. 27, 654–670.

Khan, U.A., Liu, L., Provenzano, F.A., Berman, D.E., Profaci, C.P., Sloan, R., Mayeux, R., Duff, K.E., and Small, S.A. (2014). Molecular drivers and cortical spread of lateral entorhinal cortex dysfunction in preclinical Alzheimer's disease. Nat. Neurosci. 17, 304–311.

Kilimann, I., Hausner, L., Fellgiebel, A., Filippi, M., Würdemann, T.J., Heinsen, H., and Teipel, S.J. (2017). Parallel atrophy of cortex and basal forebrain cholinergic system in mild cognitive impairment. Cereb. Cortex 27, 1841–1848.

Kolisnyk, B., Al-Onaizi, M., Soreq, L., Barbash, S., Bekenstein, U., Haberman, N., Hanin, G., Kish, M.T., Souza da Silva, J., Fahnestock, M., et al. (2017). Cholinergic surveillance over hippocampal RNA metabolism and Alzheimer's-like pathology. Cereb. Cortex 27, 3553–3567.

Kolisnyk, B., Al-Onaizi, M.A., Xu, J., Parfitt, G.M., Ostapchenko, V.G., Hanin, G., Soreq, H., Prado, M.A., and Prado, V.F. (2016). Cholinergic regulation of hnRNPA2/B1 translation by M1 muscarinic receptors. J. Neurosci. 36, 6287–6296.

Kondo, H., and Zaborszky, L. (2016). Topographic organization of the basal forebrain projections to the perirhinal, postrhinal, and entorhinal cortex in rats. J. Comp. Neurol. 524, 2503–2515.

Kriegeskorte, N., Goebel, R., and Bandettini, P. (2006). Information-based functional brain mapping. Proc. Natl. Acad. Sci. USA 103, 3863–3868.

Lewis, N.E., Schramm, G., Bordbar, A., Schellenberger, J., Andersen, M.P., Cheng, J.K., Patel, N., Yee, A., Lewis, R.A., Eils, R., et al. (2010). Large-scale in silico modeling of metabolic interactions between cell types in the human brain. Nat. Biotechnol. 28, 1279–1285.

Lin, S.C., Brown, R.E., Hussain Shuler, M.G., Petersen, C.C., and Kepecs, A. (2015). Optogenetic dissection of the basal forebrain neuromodulatory control of cortical activation, plasticity, and cognition. J. Neurosci. 35, 13896–13903.

Mattson, M.P., and Magnus, T. (2006). Ageing and neuronal vulnerability. Nat. Rev. Neurosci. 7, 278–294.

Mesulam, M.M. (2013). Cholinergic circuitry of the human nucleus basalis and its fate in Alzheimer's disease. J. Comp. Neurol. 521, 4124–4144.

Mesulam, M.M., and Geula, C. (1988). Nucleus basalis (Ch4) and cortical cholinergic innervation in the human brain: observations based on the distribution of acetylcholinesterase and choline acetyltransferase. J. Comp. Neurol. 275, 216–240.

Mesulam, M.M., Mufson, E.J., Levey, A.I., and Wainer, B.H. (1983a). Cholinergic innervation of cortex by the basal forebrain: cytochemistry and cortical connections of the septal area, diagonal band nuclei, nucleus basalis (substantia innominata), and hypothalamus in the rhesus monkey. J. Comp. Neurol. 214, 170–197.

Mesulam, M.M., Mufson, E.J., Wainer, B.H., and Levey, A.I. (1983b). Central cholinergic pathways in the rat: an overview based on an alternative nomenclature (Ch1-Ch6). Neuroscience 10, 1185–1201.

Mesulam, M.M., Mufson, E.J., and Wainer, B.H. (1986). Three-dimensional representation and cortical projection topography of the nucleus basalis (Ch4) in the macaque: concurrent demonstration of choline acetyltransferase and retrograde transport with a stabilized tetramethylbenzidine method for horseradish peroxidase. Brain Res. 367, 301–308.

Mesulam, M., Shaw, P., Mash, D., and Weintraub, S. (2004). Cholinergic nucleus basalis tauopathy emerges early in the aging-MCI-AD continuum. Ann. Neurol. 55, 815–828.

Mueller, S.G., Weiner, M.W., Thal, L.J., Petersen, R.C., Jack, C.R., Jagust, W., Trojanowski, J.Q., Toga, A.W., and Beckett, L. (2005). Ways toward an early diagnosis in Alzheimer's disease: the Alzheimer's Disease Neuroimaging Initiative (ADNI). Alzheimers Dement. 1, 55–66.

Nichols, T., Brett, M., Andersson, J., Wager, T., and Poline, J.B. (2005). Valid conjunction inference with the minimum statistic. Neuroimage 25, 653–660.

Nili, H., Wingfield, C., Walther, A., Su, L., Marslen-Wilson, W., and Kriege-skorte, N. (2014). A toolbox for representational similarity analysis. PLoS Comput. Biol. *10*, e1003553.

Parent, M., Bedard, M.A., Aliaga, A., Soucy, J.P., Landry St-Pierre, E., Cyr, M., Kostikov, A., Schirrmacher, E., Massarweh, G., and Rosa-Neto, P. (2012). PET imaging of cholinergic deficits in rats using [18F]fluoroethoxybenzovesamicol ([18F]FEOBV). Neuroimage *62*, 555–561.

Poirier, J., Delisle, M.C., Quirion, R., Aubert, I., Farlow, M., Lahiri, D., Hui, S., Bertrand, P., Nalbantoglu, J., Gilfix, B.M., and Gauthier, S. (1995). Apolipoprotein E4 allele as a predictor of cholinergic deficits and treatment outcome in Alzheimer disease. Proc. Natl. Acad. Sci. USA *92*, 12260–12264.

Prado, V.F., Roy, A., Kolisnyk, B., Gros, R., and Prado, M.A. (2013). Regulation of cholinergic activity by the vesicular acetylcholine transporter. Biochem. J. *450*, 265–274.

Raj, A., Kuceyeski, A., and Weiner, M. (2012). A network diffusion model of disease progression in dementia. Neuron *73*, 1204–1215.

Raj, A., LoCastro, E., Kuceyeski, A., Tosun, D., Relkin, N., and Weiner, M.; for the Alzheimer's Disease Neuroimaging Initiative (ADNI) (2015). Network diffusion model of progression predicts longitudinal patterns of atrophy and metabolism in Alzheimer's disease. Cell Rep. Published online January 14, 2015. https://doi.org/10.1016/j.celrep.2014.12.034.

Rivera, E.J., Goldin, A., Fulmer, N., Tavares, R., Wands, J.R., and de la Monte, S.M. (2005). Insulin and insulin-like growth factor expression and function deteriorate with progression of Alzheimer's disease: link to brain reductions in acetylcholine. J. Alzheimers Dis. *8*, 247–268.

Romberg, C., Bussey, T.J., and Saksida, L.M. (2013). Paying more attention to attention: towards more comprehensive cognitive translation using mouse models of Alzheimer's disease. Brain Res. Bull. *92*, 49–55.

Schliebs, R., and Arendt, T. (2006). The significance of the cholinergic system in the brain during aging and in Alzheimer's disease. J. Neural Transm. (Vienna) *113*, 1625–1644.

Schliebs, R., and Arendt, T. (2011). The cholinergic system in aging and neuronal degeneration. Behav. Brain Res. *221*, 555–563.

Schmitz, T.W., and Duncan, J. (2018). Normalization and the cholinergic microcircuit: a unified basis for attention. Trends Cogn. Sci. *22*, 422–437.

Schmitz, T.W., Cheng, F.H., and De Rosa, E. (2010). Failing to ignore: paradoxical neural effects of perceptual load on early attentional selection in normal aging. J. Neurosci. *30*, 14750–14758.

Schmitz, T.W., Dixon, M.L., Anderson, A.K., and De Rosa, E. (2014). Distinguishing attentional gain and tuning in young and older adults. Neurobiol. Aging *35*, 2514–2525.

Schmitz, T.W., and Spreng, R.N.; Alzheimer's Disease Neuroimaging Initiative (2016). Basal forebrain degeneration precedes and predicts the cortical spread of Alzheimer's pathology. Nat. Commun. *7*, 13249.

Seeley, W.W., Crawford, R.K., Zhou, J., Miller, B.L., and Greicius, M.D. (2009). Neurodegenerative diseases target large-scale human brain networks. Neuron *62*, 42–52.

Shaw, L.M., Vanderstichele, H., Knapik-Czajka, M., Clark, C.M., Aisen, P.S., Petersen, R.C., Blennow, K., Soares, H., Simon, A., Lewczuk, P., et al.; Alzheimer's Disease Neuroimaging Initiative (2009). Cerebrospinal fluid biomarker signature in Alzheimer's disease neuroimaging initiative subjects. Ann. Neurol. *65*, 403–413.

Spreng, R.N., and Turner, G.R. (2013). Structural covariance of the default network in healthy and pathological aging. J. Neurosci. *33*, 15226–15234.

Wang, X., Michaelis, M.L., and Michaelis, E.K. (2010). Functional genomics of brain aging and Alzheimer's disease: focus on selective neuronal vulnerability. Curr. Genomics *11*, 618–633.

Wilcox, R. (2004). Introduction to Robust Estimation and Hypothesis Testing, Second Edition (Academic Press).

Woo, C.W., Krishnan, A., and Wager, T.D. (2014). Cluster-extent based thresholding in fMRI analyses: pitfalls and recommendations. Neuroimage *91*, 412–419.

Wu, H., Williams, J., and Nathans, J. (2014). Complete morphologies of basal forebrain cholinergic neurons in the mouse. eLife *3*, e02444.

Zaborszky, L., Hoemke, L., Mohlberg, H., Schleicher, A., Amunts, K., and Zilles, K. (2008). Stereotaxic probabilistic maps of the magnocellular cell groups in human basal forebrain. Neuroimage *42*, 1127–1141.

Zaborszky, L., Csordas, A., Mosca, K., Kim, J., Gielow, M.R., Vadasz, C., and Nadasdy, Z. (2015). Neurons in the basal forebrain project to the cortex in a complex topographic organization that reflects corticocortical connectivity patterns: an experimental study based on retrograde tracing and 3D reconstruction. Cereb. Cortex *25*, 118–137.